Equivalent-Input-Disturbance-Based Dynamic Tracking Control for Soft Robots via Reduced-Order Finite-Element Models

Shijie Li, Alexandre Kruszewski, Thierry-Marie Guerra, Tran Anh-Tu Nguyen

Equivalent-Input-Disturbance Based Dynamic Tracking Control for Soft Robots Via Reduced Order Finite Element Models

Article *in* IEEE/ASME Transactions on Mechatronics · January 2022

DOI: 10.1109/TMECH.2022.3144353

CITATIONS
10

READS
389

4 authors, including:

Alexandre Kruszewski
École Centrale de Lille
99 PUBLICATIONS **2,492** CITATIONS
SEE PROFILE

Thierry-Marie Guerra
Université Polytechnique Hauts-de-France
349 PUBLICATIONS **9,873** CITATIONS
SEE PROFILE

Anh-Tu Nguyen
Université Polytechnique Hauts-de-France
140 PUBLICATIONS **2,084** CITATIONS
SEE PROFILE

Equivalent-Input-Disturbance Based Dynamic Tracking Control for Soft Robots Via Reduced Order Finite Element Models

Shijie Li, Alexandre Kruszewski, Thierry-Marie Guerra, Anh-Tu Nguyen*, *Senior Member, IEEE*

***Abstract*—This paper develops a *systematic* framework for dynamic tracking control of soft robots. To this end, we propose a new projector for the proper orthogonal decomposition algorithm to significantly reduce the large-scale robot models, obtained from finite element methods (FEM), while preserving their structure and stability properties. Such a property preservation enables an effective equivalent-input-disturbance based scheme for dynamic tracking control of elastic soft robots with various geometries and materials. The proposed control scheme is composed of three key components, *i.e.*, feedforward control, disturbance-estimator control and feedback control. To account for the trajectory reference, the feedforward action is designed from the dynamic FEM reduced-order robot model. The disturbance-estimator control action is obtained from an unknown input observer, which also provides the estimates of the reduced-states for feedback control design. The feedback gains of the observer-based controller are computed from an optimization problem under linear matrix inequality constraints. The closed-loop tracking properties are guaranteed using Lyapunov stability theory. The effectiveness of the proposed dynamic control framework has been demonstrated via both high-fidelity SOFA simulations and experimental validations, performed on two soft robots with different natures. In particular, comparative studies with state-of-the-art control methods have been also carried out to highlight the interests of the new soft robot control results. This paper is complemented with a video: `https://bit.ly/2VVwtLn`.**

***Index Terms*—Soft robots, dynamic controllers, model order reduction, finite element model, uncertainty compensation, motion control.**

I. Introduction

The emerging field of soft robotics has recently become one of the fastest growing topics in the robotic community [1]. Compared to rigid robots, soft robots have a more large-scale flexibility, deformability and adaptability to accomplish challenging tasks in interaction with humans and/or the environment [2], [3], *e.g.*, surgery, assistive medical devices, search and rescue, etc. Generally inspired by natural organisms, the motion of soft robots is realized by deformation [3], *i.e.*, in contrast to conventional rigid robots no joints are present in the structure of soft robots. Typical behaviors of soft robots, *e.g.*, bending, extension, result in infinite degrees-of-freedom (DoF) motions. Hence, developing mathematical models that reliably represent the behaviors of such infinite DoF robots still remains challenging, especially for control design purposes [4]. Moreover, the nonlinear characteristics from material properties and actuation-sensing techniques considerably limit the control performance of soft robots [5]–[7].

Up to now, a large variety of approaches have been proposed for the control issues of soft robots [6], *e.g.*, optimization based open-loop control, learning control, kinematic and dynamic model-based control, etc. Quadratic programming (QP) optimizations have been performed to numerically obtain the inverse kinematics, which can be used to compute the control action [8]–[10]. Based on a dynamic multi-body model, an iterative learning algorithm has been proposed in [11] as an open-loop control strategy for a soft spatial fluidic elastomer manipulator. These model-based control methods may lead to a heavy computational burden, especially when accurate high-dimensional models of soft robots are required for control design. To avoid this practical drawback, learning-based model-free algorithms have been developed to open-loop control the dynamic motions of soft robots [6], [12]. Although open-loop control strategies can be applied to various types of soft robots, however such control strategies are only effective under quasi-static assumptions, *i.e.*, with slow motions. Moreover, open-loop control suffers a lack of performance and robustness in presence of modeling uncertainty or disturbances.

Feedback control has been proved as a solution to improve the closed-loop behaviors of soft robots [13]. Closed-loop controllers can be classified into two categories, *i.e.*, kinematic control and dynamic control. For kinematic control, a data-driven model has been developed to design a disturbance observer based controller for a soft crawling robot in [14]. Based on visual servoing, an online learning kinematic algorithm has been proposed in [15] for soft robots. Using a piecewise constant curvature (PCC) model, the authors in [16] have developed an adaptive kinematic controller for soft robot manipulators in constrained environments. Hyatt et *al.* have proposed a kinematic controller using soft-robot joint estimation, kinematic calibration, and visual servoing to deal with the uncertainty in forward kinematics [17]. From the knowledge of the Jacobian, describing the relationship between the end-effector position and the control inputs, proportional-integral-derivative (PID) control has been designed for tracking tasks of soft robots [18], [19]. Relying on the steady-state assumption, in many practical situations kinematic control methods cannot provide sufficient

S. Li, A.-T. Nguyen and T.-M. Guerra are with the LAMIH laboratory, UMR CNRS 8201, Université Polytechnique Hauts-de-France, Valenciennes, France. S. Li is also with the DEFROST team, INRIA, CRIStAL laboratory, UMR CNRS 9189, Villeneuve d'Ascq, France. A.-T. Nguyen is also with the INSA Hauts-de-France, Valenciennes, France (e-mail: {shijie.li, tnguyen,guerra}@uphf.fr).

A. Kruszewski is with the DEFROST team, INRIA, University of Lille, Centrale Lille, CRIStAL laboratory, UMR CNRS 9189, Villeneuve d'Ascq, France (e-mail: alexandre.kruszewski@centralelille.fr).

*Corresponding author: Anh-Tu Nguyen (nguyen.trananhtu@gmail.com).

performance [19], [20], *e.g.*, precision, rapidity, robustness, especially for high speed tracking tasks. This motivates the development of dynamic controllers. Using a modified Lagrange polynomial series-solution, the authors in [21] have derived the Cosserat rod static and Lagrangian dynamic model of a continuum manipulator, which enables to design a nonlinear impedance and configuration feedback controller. An extended PCC-based formulation, linking a soft robot to a classic rigid-bodied serial manipulator, has been recently proposed in [22] for dynamic tracking control of planar soft robots interaction with environments. Note that PCC-based methods are generally limited to beam-like robots with bending deformations, and seem difficult to be adapted to a wide range of soft robots [23]. Model predictive control (MPC) has been proposed in [24], [25] for the tracking control of soft robots. Note that the control performance of MPC methods strongly depends on the modeling accuracy of the considered robots [26]. A tracking controller, combining a low-gain feedback component and a learning-based feedforward action, has been proposed in [27] for articulated soft robots. However, the performance of the learned control action is only suited for a predefined desired trajectory and stiffness parameter profile. Reinforcement learning control method [20] and a model-based adaptive control method [28] have been also developed for various soft robots.

Despite a considerable research effort, dynamic control design still remains a challenging issue in soft robotics [6], [22]. Most of existing approaches are only suitable for some classes of robots with specific geometries. Dynamic control based on finite element models of soft robots has been recently shown as a promising solution for this major drawback [13]. Finite element methods (FEM) require a spatial discretization of the structure into a mesh [29], which can thus handle a large class of elastic soft robots with different geometries and materials [30]. However, the finer is the mesh the better is the model accuracy, as illustrated in Fig. 1. Then, a reliable robot model can be only obtained with a very large number of variables. The *large-scale* nature of soft robot models implies technical challenges in designing dynamic controllers with conventional control tools [31]. Moreover, the obtained controllers cannot be directly applied to soft robots in practice. Hence, model order reduction (MOR) is useful for FEM-based dynamic control design [32], [33].

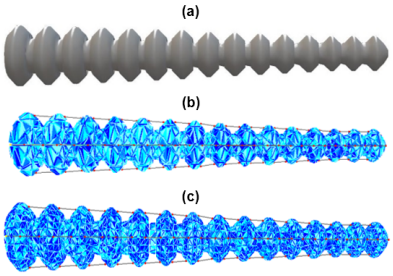

Fig. 1. Illustrations of FEM modeling for a Trunk robot. (a) Visual model. (b) FEM model with a coarse mesh. (c) FEM model with a medium-size mesh.

Motivated by the above technical issues, this paper proposes a *systematic* framework for dynamic reference tracking control of soft robots. To this end, we modify the proper orthogonal decomposition (POD) method used in [13], [33] to significantly reduce the order of FEM soft robot models while preserving their structure and stability properties. As will be shown, the structure preservation enables a more effective dynamic control scheme, especially in case of uncertainty and disturbances. The proposed control scheme is formed with three main components, *i.e.*, feedforward control, disturbance-estimator control and feedback control. Using the dynamic FEM reduced-order model, the feedforward action is designed to account for the reference trajectory whereas the disturbance-estimator control is designed to compensate the modeling uncertainty. The observer-based feedback control is designed to guarantee a desired tracking performance, specified by an optimized $\ell_\infty-$gain and a predefined linear matrix inequality (LMI) region of the closed-loop robot system. Specifically, our main contributions can be summarized as follows.

- Compared to the related works [13], [33], we propose a new projector for the POD reduction method. Then, the reduced-order models of soft robots can be obtained while preserving the structure and stability properties, which is crucial to design an effective feedback-feedforward control scheme in presence of modeling uncertainties.
- Exploiting the equivalent-input-disturbance (EID) concept [34], [35] for a specific mechanical model structure of soft robots, we develop an FEM model-based control framework to achieve high-precision tracking tasks despite of *unknown* uncertainties and disturbances. The closed-loop performance is rigorously guaranteed by Lyapunov stability theory, which is not the case of most of existing results on soft robotics control.
- High-fidelity SOFA simulations and experimental validations have been performed on two soft robots with different natures to demonstrate the effectiveness of the proposed control framework.

Notation. $\mathbb{R}$ is the set of real numbers. For a matrix X, $X^\top$ denotes its transpose, $X \succ 0$ means that X is symmetric positive definite, $\mathrm{He}(X) = X + X^\top$, $\mathrm{Sym}(X) = X - X^\top$, and $\lambda_{\min}(X)$, $\lambda_{\max}(X)$ denotes respectively the minimal and maximal eigenvalues of a symmetric matrix X. $\mathrm{diag}(X_1, X_2)$ denotes a block-diagonal matrix composed of matrices X_1 and X_2. I is the identity matrix of appropriate dimension. For a vector $x \in \mathbb{R}^n$, we denote its 2-norm as $\|x\| = \sqrt{x^\top x}$. For a function $f : \mathbb{R} \to \mathbb{R}^n$, its $\ell_\infty-$norm is defined as $\|f\|_\infty = \sup_{t\in\mathbb{R}} \|f(t)\|$, and $\mathscr{B}_\infty$ is the set of bounded functions f. The symbol '$\star$' stands for the terms deduced by symmetry in symmetric block matrices. The argument of a function is omitted when its meaning is clear.

II. Modeling of Soft Robots

This section provides a procedure to obtain control-based models for large-scale soft robotics systems.

A. From FEM Modeling to State-Space Representation

For the modeling of soft robots, FEM method is used to approximate the infinite-dimensional model by subdividing it into a large amount of tiny elements [29]. The resulting discretized model has the number of degrees of freedom proportional to the

number of elements. The dynamics of a deformable soft robot can be described as follows [4]:

$$\mathcal{M}(q)\ddot{q} = \mathcal{P}(q) - \mathcal{F}(q,\dot{q}) + \mathcal{H}(q)u, \tag{1}$$

where $q \in \mathbb{R}^n$ is the displacement vector, $\dot{q} \in \mathbb{R}^n$ is the velocity vector, $u \in \mathbb{R}^m$ is the control input, $\mathcal{M}(q) \in \mathbb{R}^{n\times n}$ is the inertia matrix, $\mathcal{F}(q,\dot{q})$ represents the internal elastic forces of soft robots, $\mathcal{P}(q)$ represents known external forces, $\mathcal{H}(q)$ is the control input matrix. We consider the case that $\mathcal{P}(q)$ only contains the gravity force, and the mass distribution does not change over time. Hence, the positive definite matrices $\mathcal{P}(q) = P$ and $\mathcal{M}(q) = M$ are constant. Without loss of generality, assume that the tracking control of soft robots is performed around an equilibrium point, defined as $(q_0, \dot{q}_0) = (0,0)$ and $u_0 = 0$. Then, it follows from (1) that

$$P - \mathcal{F}(0,0) = 0. \tag{2}$$

Moreover, around the equilibrium point the internal force $\mathcal{F}(q,\dot{q})$ can be approximated as

$$\mathcal{F}(q,\dot{q}) \approx \mathcal{F}(0,0) + \mathcal{K}(q,\dot{q})q + \mathcal{D}(q,\dot{q})\dot{q}. \tag{3}$$

The compliance matrix $\mathcal{K}(q,\dot{q})$ and the damping matrix $D(q,\dot{q})$ are respectively defined as

$$\mathcal{K}(q,\dot{q}) = \frac{\partial \mathcal{F}(q,\dot{q})}{\partial q}, \quad \mathcal{D}(q,\dot{q}) = \frac{\partial \mathcal{F}(q,\dot{q})}{\partial \dot{q}}.$$

Substituting (2) and (3) into (1), the linearized FEM model of the soft robot can be obtained as

$$M\ddot{q} \approx -\mathcal{K}(0,0)q - \mathcal{D}(0,0)\dot{q} + \mathcal{H}(0)u. \tag{4}$$

For conciseness, we denote $K = \mathcal{K}(0,0)$, $D = \mathcal{D}(0,0)$ and $H = \mathcal{H}(0)$. Then, system (4) can be rewritten in the state-space form

$$\dot{x} = Ax + Bu, \quad y = Cx, \tag{5}$$

where $x = \begin{bmatrix}\dot{q}^\top & q^\top\end{bmatrix}^\top \in \mathbb{R}^{2n}$. The matrices $A \in \mathbb{R}^{2n\times 2n}$ and $B \in \mathbb{R}^{2n\times m}$ are large-scale sparse, defined as

$$A = \begin{bmatrix} -M^{-1}D & -M^{-1}K \\ I & 0 \end{bmatrix}, \quad B = \begin{bmatrix} M^{-1}H \\ 0 \end{bmatrix}. \tag{6}$$

The system output $y \in \mathbb{R}^p$ represents the coordinates of the robot end-effector.

Remark 1. The compliance matrix K and the damping matrix D are symmetric positive definite. Due to the large-scale feature of system (5), *i.e.*, $n > 3000$, and the scattered connection between local neighbor elements in FEM modeling, these matrices are also sparse.

B. Model Order Reduction for Soft Robots

Many MOR methods have been proposed for large-scale systems, *e.g.*, singular value decomposition (SVD), moment matching [36]. As an SVD-based method, POD enables an effective model order reduction with *a priori* error bound. Moreover, in contrast to most of existing MOR methods, POD algorithms can be directly applied to large-scale nonlinear systems [37]. Hence, POD has been shown as a suitable MOR method for soft robots [13]. Exploiting the data interdependencies within snapshots, *i.e.*, response of the system states with respect to excitation signals, this data-based method significantly reduces the system state dimension through an orthogonal projection operator $T_r^* \in \mathbb{R}^{2n\times 2l}$, defined as

$$\begin{bmatrix} x_r \\ x_{\bar{r}} \end{bmatrix} = \begin{bmatrix} T_r^* \\ T_{\bar{r}}^* \end{bmatrix} x, \tag{7}$$

where $x_r \in \mathbb{R}^{2l}$ is the reduced state vector with $l \ll n$, $x_{\bar{r}}$ is the neglected state vector, and $T_{\bar{r}}^*$ is the orthogonal complement of matrix T_r^*. Since the POD method only requires SVD operations to obtain the projector, this method is computationally efficient for *a priori* given snapshots [37].

Despite its effectiveness in reducing the order of system (5) for control design, the POD projection (7) generally does not allow preserving the stability and the *mechanical* structure properties of this large-scale system [38], which are crucial for the proposed EID-based control scheme. To overcome this drawback, we propose a modified POD projection taking into account the specific matrix structures of system (5). To this end, only the displacement vector is projected into the low-dimension space. Then, the reduced velocity vector can be obtained with the same projector matrix. As a result, we have

$$x_r = \begin{bmatrix} \dot{q}_r \\ q_r \end{bmatrix} = \begin{bmatrix} T & 0 \\ 0 & T \end{bmatrix} \begin{bmatrix} \dot{q} \\ q \end{bmatrix} = T_r x. \tag{8}$$

Applying the proposed projector (8) to system (5), the following approximated reduced-order model can be obtained:

$$\begin{aligned} \dot{x}_r &= A_r x_r + B_r u + T_r A T_{\bar{r}}^\top x_{\bar{r}}, \\ y &= C_r x_r, \end{aligned} \tag{9}$$

where $T_{\bar{r}}$ is the orthogonal complement of matrix T_r, and

$$\begin{aligned} A_r &= T_r A T_r^\top = \begin{bmatrix} -TM^{-1}DT^\top & -TM^{-1}KT^\top \\ I & 0 \end{bmatrix}, \\ B_r &= T_r B = \begin{bmatrix} TM^{-1}H \\ 0 \end{bmatrix}, \quad C_r = CT_r^\top. \end{aligned}$$

The accuracy of the POD reduced-order models depends on the decay rate of the singular values of the snapshots [33]. Fig. 2(a) depicts the evolution of the singular values corresponding to the position snapshots of the Trunk robot discussed in Section V. As shown in Fig. 2(b), a fast decay of singular values is clearly observed for the first four values, which represent more than 95% of the singular values of the 3324-state FEM robot model. Then, the POD method with the proposed projector (8) can significantly reduce the number of the state variables, *i.e.*, from 3324 to 4 states, while keeping a good modeling quality for dynamic control purposes.

Remark 2. With the proposed POD projector (8), the matrix structures are preserved between system (6) and its reduced-order counterpart (9), *i.e.*, the parameters are only involved in the upper-half of the state-space matrices. As shown in the sequel, this enables an effective EID-based control framework to compensate the modeling uncertainty for tracking performance improvements. This MOR property preservation has not been yet exploited for dynamic control of soft robots.

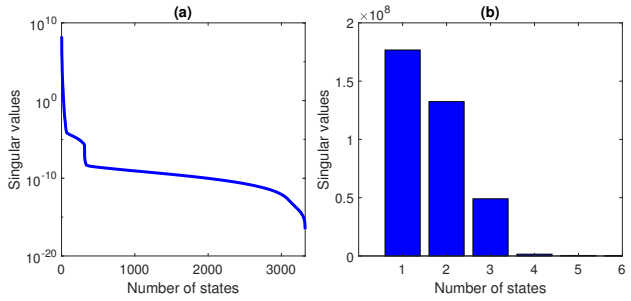

Fig. 2. Singular values of the position snapshots of a Trunk robot. (a) Evolution of the singular values. (b) Six first singular values.

1) Model Error Analysis: We consider uncertainty in the knowledge of compliance, damping and control matrices as

$$\hat{K} = K + \Delta K, \quad \hat{D} = D + \Delta D, \quad \hat{H} = H + \Delta H,$$

where $\hat{K}$, $\hat{D}$, $\hat{H}$ are the estimations, K, D, H the real values, and ΔK, ΔD, ΔH the uncertainties. Since the system structure is preserved, these uncertain terms are taken into account in the reduced-order model (9) as

$$\dot{x}_r = \hat{A}_r x_r + \hat{B}_r u + T_r \hat{A} T_{\bar{r}}^\top x_{\bar{r}}, \tag{10}$$

with

$$\hat{A}_r = A_r + \Delta A_r, \quad \hat{B}_r = B_r + \Delta B_r,$$
$$\hat{A} = A + \Delta A, \quad \Delta A = \begin{bmatrix} -M^{-1}\Delta D & -M^{-1}\Delta K^\top \\ 0 & 0 \end{bmatrix},$$
$$\Delta A_r = T_r \Delta A T_r^\top, \quad \Delta B_r = \begin{bmatrix} TM^{-1}\Delta H \\ 0 \end{bmatrix}.$$

Note that due to the specific upper-half structures of matrices B_r, ΔA_r and ΔB_r, the following matrix decompositions can be performed:

$$\Delta A_r = B_r B_r^\dagger \Delta \bar{A}_r, \quad \Delta B_r = B_r B_r^\dagger \Delta \bar{B}_r, \tag{11}$$

where $B_r^\dagger = \left(B_r^\top B_r\right)^{-1} B_r^\top$ is the pseudo-inverse of B_r, and

$$\Delta \bar{A}_r = \begin{bmatrix} -TM^{-1}\Delta D T^\top & -TM^{-1}\Delta K T^\top \end{bmatrix},$$
$$\Delta \bar{B}_r = TM^{-1}\Delta H.$$

Let us define a *lumped* disturbance as

$$d_l = B_r^\dagger \Delta \bar{A}_r x_r + B_r^\dagger \Delta \bar{B}_r u. \tag{12}$$

Moreover, to take into account the neglected state dynamics for the control design, we can decompose

$$T_r \hat{A} T_{\bar{r}}^\top x_{\bar{r}} = B_r d_{\ddot{q}} + B_{\bar{r}} d_{\dot{q}}. \tag{13}$$

where $B_{\bar{r}}$ is an orthogonal complement of B_r. Note that the disturbance $d_{\ddot{q}}$ (respectively $d_{\dot{q}}$) corresponds to the neglected dynamics related to the acceleration $\ddot{q}$ (respectively velocity $\dot{q}$). From (11), (12) and (13), the uncertain reduced-order model (10) can be represented as

$$\begin{aligned} \dot{x}_r &= A_r x_r + B_r(u + d_e) + B_{\bar{r}} d_{\dot{q}}, \\ y &= C_r x_r, \end{aligned} \tag{14}$$

with $d_e = d_{\ddot{q}} + d_l$.

2) Transformation of Generalized Coordinates: Although the proposed POD projector (8) allows preserving the structures of the state-space matrices, the state variables of the reduced-order model (9) no longer represent the displacement and the velocity of soft robots in the Cartesian coordinates. These new state variables can be considered as *generalized* coordinates. Hence, a coordinate transformation between generalized coordinates and Cartesian coordinates is required to design an effective model-based feedforward control action. Indeed, for trajectory tracking only the robot outputs are required to track their corresponding reference signals, directly defined in the Cartesian coordinate system, *i.e.*, a reference model is generally not available in the generalized coordinate system for control design as in [13].

Since the output of soft robots only includes the coordinates of the end-effectors, it follows from (9) that

$$y = C_r x_r = C_g q_r,$$

with $C_r = \begin{bmatrix} 0 & C_g \end{bmatrix}$ and $C_g \in \mathbb{R}^{p \times l}$. Then, if the MOR is performed with $p = l$, then the proposed POD method can provide a full-rank matrix C_g. Hence, for any arbitrary desired trajectory r in Cartesian coordinates, the corresponding trajectory r_g in generalized coordinates can be defined as $r_g = C_g^{-1} r$. As shown in (17), this relation allows for a full use of the dynamic FEM reduced-order model (14) of soft robots to design an effective feedforward control action.

III. Tracking Control Problem Formulation

This section formulates the tracking control problem of soft robots. To this end, we define the tracking error in generalized coordinates as $e = x_r - r_g$. Then, the tracking error dynamics can be defined from (14) as

$$\dot{e} = A_r e + B_r(u + d_e) + A_r r_g - \dot{r}_g + B_{\bar{r}} d_{\dot{q}}. \tag{15}$$

To deal with the modeling uncertainty and improve the tracking control performance of soft robots, we propose a feedback-feedforward control scheme composed of three components as

$$u = u_{ff} + u_{dc} + u_{fb}, \tag{16}$$

where u_{ff} is the feedforward control, u_{dc} is the disturbance-estimator based control, and u_{fb} is the feedback control. The proposed tracking control scheme is illustrated in Fig 3.

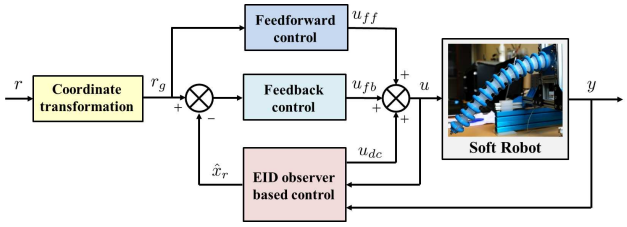

Fig. 3. EID observer-based tracking control structure for soft robots.

1) Feedforward Control: The feedforward control u_{ff} accounts for the affect of the reference signal r_g, considered as a *known* disturbance, on the closed-loop system. Hence, this control action is designed such that

$$B_r u_{ff} = -(A_r r_g - \dot{r}_g). \tag{17}$$

The feedforward action can be designed from (17) as

$$u_{ff} = -B_r^{\dagger}(A_r r_g - \dot{r}_g). \tag{18}$$

2) Disturbance-Estimator Based Control: The lumped disturbance d_e includes the nonlinearity and modeling uncertainty. Note from (15) that d_e enters in the system dynamics via the same channel as the input u, *i.e.*, matching disturbance. Then, the disturbance-estimator based control can be designed as follows:

$$u_{dc} = -\hat{d}_{ef}, \tag{19}$$

where $\hat{d}_{ef}$ is an estimate of the *filtered* signal d_{ef} of the lumped disturbance d_e. To estimate this disturbance, we assume that d_e is of low-frequency, whose dynamics can be efficiently captured using a *piecewise* second-order polynomial signal [39]. Note that this assumption is suitable due to the low-frequency behaviors of soft robots. Moreover, inspired by the EID approach [34], we integrate a low-pass filter with a time constant T_f of the form

$$\mathbf{F}(s) = \frac{1}{1+T_f s} I, \tag{20}$$

where s is the Laplace variable, to limit the angular-frequency band of the disturbance estimate as shown in Fig. 3. Then, the disturbance model is given as

$$\dot{d} = Jd, \tag{21}$$

with

$$d = \begin{bmatrix} d_{ef} \\ d_e \\ \dot{d}_e \end{bmatrix}, \quad J = \begin{bmatrix} -\frac{1}{T_f} I & \frac{1}{T_f} I & 0 \\ 0 & 0 & I \\ 0 & 0 & 0 \end{bmatrix}.$$

From (14) and (21), we propose the following Luenberger-like unknown input observer to estimate *simultaneously* the state x_r and the unknown disturbance d_e:

$$\begin{aligned} \dot{\hat{x}}_r &= A_r \hat{x}_r + B_r(u + \hat{d}_e) + L_x(y - \hat{y}), \\ \dot{\hat{d}} &= J\hat{d} + L_d(y - \hat{y}), \\ \hat{y} &= C_r \hat{x}_r, \end{aligned} \tag{22}$$

where $\hat{d}$ is the estimate of d, the observer gains $L_x \in \mathbb{R}^{2l \times p}$ and $L_d \in \mathbb{R}^{3m \times p}$ are to be designed.

Remark 3. The filter $\mathbf{F}(s)$ in (20) is integrated into the unknown input observer (22) to offer a degree of freedom to regulate the angular-frequency band for disturbance rejection. Then, the value of T_f can be selected as

$$T_f \in \left[\frac{1}{10\omega_r}, \frac{1}{5\omega_r} \right],$$

where ω_r is the highest angular frequency selected for disturbance rejection purposes [34].

The estimation error dynamics can be defined from (14), (21) and (22) as follows:

$$\dot{\varepsilon} = (A_o - L_o C_o)\varepsilon + B_{od} d_{\dot{q}}, \tag{23}$$

with

$$A_o = \begin{bmatrix} A_r & \tilde{B}_r \\ 0 & J \end{bmatrix}, \quad B_{od} = \begin{bmatrix} B_{\bar{r}} \\ 0 \end{bmatrix}, \quad \varepsilon = \begin{bmatrix} x_r - \hat{x}_r \\ d - \hat{d} \end{bmatrix},$$
$$L_o = \begin{bmatrix} L_x^{\top} & L_d^{\top} \end{bmatrix}^{\top}, \quad \tilde{B}_r = \begin{bmatrix} B_r & 0 \end{bmatrix}, \quad C_o = \begin{bmatrix} C_r & 0 \end{bmatrix}.$$

3) Feedback Control: The feedback control aims at guaranteeing the closed-loop stability and improving the steady-state tracking performance. To this end, we consider the following proportional-integral control law:

$$u_{fb} = K_p(\hat{x}_r - r_g) + K_i e_i, \tag{24}$$

where $K_p \in \mathbb{R}^{m \times 2l}$ and $K_i \in \mathbb{R}^{m \times p}$ are the feedback gains to be designed, and

$$\dot{e}_i = C_r(x_r - r_g).$$

With u_{ff}, u_{dc} and u_{fb} respectively defined in (18), (19) and (24), substituting the control expression (16) into system (15), the tracking error dynamics can be represented as

$$\dot{\xi} = (A_c + B_c K_c)\xi + B_o \varepsilon + B_{cd} d_{\dot{q}}, \tag{25}$$

where

$$\xi = \begin{bmatrix} e^{\top} & e_i^{\top} \end{bmatrix}^{\top}, \quad A_c = \begin{bmatrix} A_r & 0 \\ C_r & 0 \end{bmatrix}, \quad B_c = \begin{bmatrix} B_r \\ 0 \end{bmatrix},$$
$$K_c = \begin{bmatrix} K_p & K_i \end{bmatrix}, \quad B_o = \begin{bmatrix} -B_r K_p & 0 \\ 0 & 0 \end{bmatrix}, \quad B_{cd} = \begin{bmatrix} B_{\bar{r}} \\ 0 \end{bmatrix}.$$

The extended closed-loop system can be defined from (23) and (25) as

$$\dot{\tilde{x}} = \begin{bmatrix} \bar{A}_c & B_o \\ 0 & \bar{A}_o \end{bmatrix} \tilde{x} + \begin{bmatrix} B_{cd} \\ B_{od} \end{bmatrix} d_{\dot{q}}, \tag{26}$$

where $\tilde{x} = \begin{bmatrix} \xi^{\top} & \varepsilon^{\top} \end{bmatrix}^{\top}$, and

$$\bar{A}_c = A_c + B_c K_c, \quad \bar{A}_o = A_o - L_o C_o.$$

Since we focus on the tracking control, the performance output associated to system (26) is the position tracking error, *i.e.*, $z = e = \tilde{C}_r \xi$, with $\tilde{C}_r = \begin{bmatrix} C_r & 0 \end{bmatrix}$. Hence, one has

$$z = F\tilde{x}, \quad F = \begin{bmatrix} \tilde{C}_r & 0 \end{bmatrix}. \tag{27}$$

To specify the performance of the closed-loop system, we exploit the concept of $\mathscr{D}-$stability [40] to design both the observer (22) and the feedback controller (24). To this end, we consider an LMI region $\mathscr{D}(r, \theta, \alpha)$ defined as a subset of the left-half complex plane to guarantee minimum decay rate α, a minimum damping ratio $\zeta = \cos(\theta)$ and a maximum undamped natural frequency $\omega_d = r\sin(\theta)$. The following lemma guarantees the $\mathscr{D}-$stability of a matrix $\mathbf{A}$.

Lemma 1 ([40])**.** All the eigenvalues of $\mathbf{A}$ are located inside the region $\mathscr{D}(r, \theta, \alpha)$ if and only if there exists a symmetric positive definite matrix $\mathbf{X}$ such that

$$\begin{aligned} &\mathbf{A}^{\top}\mathbf{X} + \mathbf{X}\mathbf{A} + 2\alpha\mathbf{X} \prec 0, \\ &\begin{bmatrix} -r\mathbf{X} & \mathbf{A}\mathbf{X} \\ \star & -r\mathbf{X} \end{bmatrix} \prec 0, \\ &\begin{bmatrix} \sin(\theta)\left(\mathbf{A}\mathbf{X} + \mathbf{X}\mathbf{A}^{\top}\right) & \cos(\theta)\left(\mathbf{A}\mathbf{X} - \mathbf{X}\mathbf{A}^{\top}\right) \\ \star & \sin(\theta)\left(\mathbf{A}\mathbf{X} + \mathbf{X}\mathbf{A}^{\top}\right) \end{bmatrix} \prec 0. \end{aligned}$$

Hereafter, we propose an effective solution for the following observer-based feedback control problem.

Problem 1. Consider two LMI regions $\mathscr{D}_c(r_c, \theta_c, \alpha_c)$ and $\mathscr{D}_o(r_o, \theta_o, \alpha_o)$. Determine the control gain K_c (respectively the observer gain L_o) such that the poles of the dynamic matrix

$\bar{A}_c$ (respectively $\bar{A}_o$) remain inside the region $\mathscr{D}_c(r_c, \theta_c, \alpha_c)$ (respectively $\mathscr{D}_o(r_o, \theta_o, \alpha_o)$). Moreover, the extended system (26) satisfies the following closed-loop properties.

(P1) For $d_{\dot{q}}(t) = 0$, $\forall t \geq 0$, system (26) is *exponentially* stable with a decay rate $\alpha > 0$. For any initial condition $\tilde{x}(0)$ and any bounded disturbance $d_{\dot{q}}(t) \in \mathscr{B}_\infty$, there exists a bound $\eta(\tilde{x}(0), \|d_{\dot{q}}\|_\infty)$ such that

$$\tilde{x}(t) \leq \eta(\tilde{x}(0), \|d_{\dot{q}}\|_\infty), \quad t \geq 0.$$

(P2) For $\forall \tilde{x}(0)$ and $\forall d_{\dot{q}}(t) \in \mathscr{B}_\infty$, we have

$$\lim_{t\to\infty} \sup \|z\| \leq \gamma \|d_{\dot{q}}\|_\infty, \quad \gamma > 0, \tag{28}$$

where the $\ell_\infty-$gain is specified in Theorem 1.

Remark from (27) and (28) that a smaller value of the $\ell_\infty-$gain γ leads to a better tracking control performance.

IV. EID-Based Output Feedback Tracking Control

This section provides conditions to design both the unknown input observer (22) and the feedback control law (24) satisfying the closed-loop specifications in Problem 1.

Theorem 1. Consider the closed-loop system (26) and two LMI regions $\mathscr{D}_c(r_c, \theta_c, \alpha_c)$ and $\mathscr{D}_o(r_o, \theta_o, \alpha_o)$. If there exist symmetric positive definite matrices $X \in \mathbb{R}^{(2l+p)\times(2l+p)}$, $Q \in \mathbb{R}^{(2l+3m)\times(2l+3m)}$, matrices $M \in \mathbb{R}^{m\times(2l+p)}$, $N \in \mathbb{R}^{(2l+3m)\times p}$, and positive scalars μ, ν such that the optimization problem (29) is feasible.

$$\text{minimize} \quad \mu + \nu, \tag{29}$$

subject to

$$\mathrm{He}\begin{bmatrix} \mathscr{A}_o + \alpha_c Q & QB_{od} \\ 0 & -\alpha_c \nu I \end{bmatrix} \prec 0, \tag{30}$$

$$\mathrm{He}(\mathscr{A}_c + \alpha_c X) \prec 0, \tag{31}$$

$$\begin{bmatrix} -r_c X & \mathscr{A}_c \\ \star & -r_c X \end{bmatrix} \prec 0, \tag{32}$$

$$\begin{bmatrix} s_{\theta_c}\mathrm{He}(\mathscr{A}_c) & c_{\theta_c}\mathrm{Sym}(\mathscr{A}_c) \\ \star & s_{\theta_c}\mathrm{He}(\mathscr{A}_c) \end{bmatrix} \prec 0, \tag{33}$$

$$\mathrm{He}(\mathscr{A}_o + \alpha_o Q) \prec 0, \tag{34}$$

$$\begin{bmatrix} -r_o Q & \mathscr{A}_o \\ \star & -r_o Q \end{bmatrix} \prec 0, \tag{35}$$

$$\begin{bmatrix} s_{\theta_o}\mathrm{He}(\mathscr{A}_o) & c_{\theta_o}\mathrm{Sym}(\mathscr{A}_o) \\ \star & s_{\theta_o}\mathrm{He}(\mathscr{A}_o) \end{bmatrix} \prec 0, \tag{36}$$

$$\begin{bmatrix} X & 0 & X\tilde{C}_r^\top \\ \star & Q & 0 \\ \star & \star & \mu I \end{bmatrix} \succeq 0, \tag{37}$$

with

$$\begin{aligned} &\mathscr{A}_c = A_c X + B_c M, \quad &&\mathscr{A}_o = QA_o - NC_o, \\ &c_{\theta_c} = \cos(\theta_c), &&s_{\theta_c} = \sin(\theta_c), \\ &c_{\theta_o} = \cos(\theta_o), &&s_{\theta_o} = \sin(\theta_o). \end{aligned}$$

Then, the feedback observer-based controller (24) is such that the closed-loop properties specified in Problem 1 are satisfied with a guaranteed $\ell_\infty-$gain $\gamma = \sqrt{\nu\mu}$. Furthermore, the control and observer gains are respectively given by

$$K_c = MX^{-1}, \quad L_o = Q^{-1}N. \tag{38}$$

Proof. The proof is postponed to Appendix A. □

Remark 4. The design procedure in Theorem 1 is recast as a convex optimization problem under LMI constraints. Here, the control gain K_c and observer gain L_o can be effectively computed using YALMIP toolbox and SeDuMi solver [41].

Remark 5. The LMI region $\mathscr{D}_c(r_c, \theta_c, \alpha_c)$ is defined to represent the dominant low-frequency dynamics of soft robots. Moreover, the damping ratio should be chosen as small as possible to avoid oscillatory behaviors of the closed-loop robot systems. However, without restrictive constraints, the LMI region $\mathscr{D}_o(r_o, \theta_o, \alpha_o)$ should be specified to guarantee a fast convergence of the estimation error dynamics (23).

V. Illustrative Results and Evaluations

This section presents the control results obtained with both FEM-based simulations and realtime experiments. To highlight the *systematic* feature of the proposed tracking control method, we consider two different silicone soft robots for validations: Diamond robot and Trunk robot, whose physical prototypes are described in [9].

A. FEM-Based Validations with Diamond Robot

The Diamond robot has four soft legs, which are actuated by cables as depicted in Fig. 4. This cable-driven robot can be considered as a soft version of parallel robots. The movement of the Diamond robot is realized through a combination of bending and squeezing of its four legs. Hence, most of the PCC-based approaches [23] are no longer suitable for *dynamic* modeling and control of such a soft robot. The weight of the Diamond robot is 0.5 [kg] and its height is 110 [mm] in the initial position. The material parameters of this soft robot are obtained through experiments. Then, the FEM model of the Diamond robot can be derived with 1570 nodes, leading to 9420 state variables. This high-fidelity FEM model is implemented in the SOFA open-source simulation platform [4] for validations. Note that the modeling error between FEM-based model and the real robot is less than 10% in a workspace of $40 \times 40 \times 20$ [mm^3] around the rest position of the robot [8]. For control design, a six-order dynamical model of the Diamond robot can be obtained with the proposed POD model reduction method. The control algorithms are implemented in MATLAB/SIMULINK environment. This SIMULINK-SOFA co-simulation environment allows reducing significantly the costs related to not only the design but also the realtime validation of complex soft robots. More details on the plugin SoftRobots for the SOFA Framework with related publications can be found at the address: https://project.inria.fr/softrobot.

For the tracking control of the Diamond robot, we consider spiral trajectories of the form

$$x(t) = 15\cos(\omega t), \; y(t) = 15\sin(\omega t), \; z(t) = 110 + t, \tag{39}$$

with $\omega = 1$ [rad/s] for a fast trajectory tracking, and $\omega = 0.33$ [rad/s] for a slow trajectory tracking. This trajectory is defined within the cylindrical workspace of the Diamond robot. To evaluate the control robustness performance with respect to the modeling errors, we consider two test scenarios, *i.e.*, *without* and

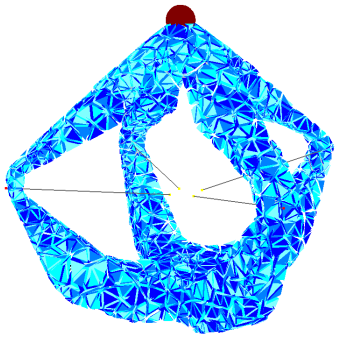

Fig. 4. FEM-based schematic of the Diamond robot. The red point represents the end-effector and the gray lines represent the driving cables.

with uncertainty on Young's modulus. This latter characterizes the *softness* property of the silicone material, *i.e.*, a softer material leads to a stronger oscillatory response in the open loop. Moreover, a comparison between the following FEM-based control methods is performed to demonstrate the effectiveness of the new control method:

- Method 1: Inverse kinematics based QP control [8], [10].
- Method 2: Jacobian-based PID control [18], [19].
- Method 3: Proposed EID-based control.

For Method 1, the QP-based controller is composed of an PI controller and an QP solver. The PI controller aims at providing a desired action of the robot end-effector whereas the QP solver computes the actuation control through an inverse kinematic optimization. The details on the QP-based control architecture and the related tuning methods can be found in [10]. For Method 2, the PID controller is defined as

$$u(t) = \mathscr{J}^{-1}\left(K_p e(t) + K_i \int e(t)dt + K_d \dot{e}(t)\right),$$

where $\mathscr{J}$ is the Jacobian matrix of the soft robot, and K_p, K_i, K_d are the PID control gains. Note that the Jacobian matrices of soft robots can be directly obtained with SOFA platform for control design. Note also that due to the low resonant frequency characteristics of soft robots, the ranges of the PID control gains are quite narrow to avoid aggressive closed-loop behaviors. Moreover, in this work the control design is only performed with reduced-order linear systems. Then, the PID controllers designed in both Method 1 and Method 2 can be empirically fine-tuned, *e.g.*, using the well-known Ziegler–Nichols method.

1) Scenario 1 [Without Uncertainty on Young's Modulus]: For this test scenario, the Young's modulus of the FEM simulation model and the FEM control-based model of the Diamond robot are both set to 150 [KPa], *i.e.*, no mismatch between two FEM models. The slow trajectory tracking is shown in Fig. 5. The feedforward action of the proposed controller and the inverse kinematic control of Method 1 allow for a better tracking performance during the steady-state phase compared to the PID controller. Observe in Fig. 6 that the drawbacks of Methods 1 and 2 become much more clear with a fast trajectory tracking in comparison to the EID-based method, *i.e.*, the dynamic response of the QP-based controller is degraded and the steady-state tracking error induced by the PID controller increases.

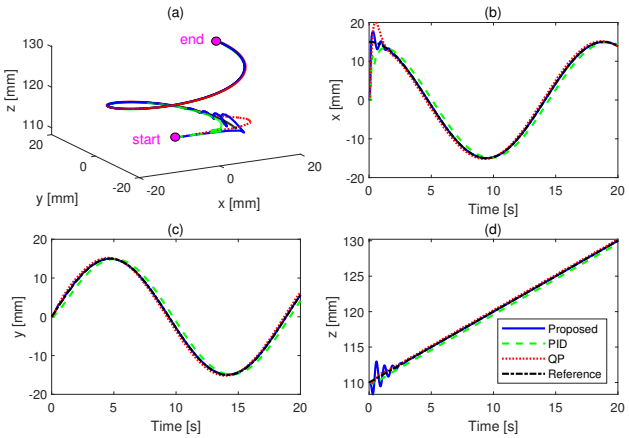

Fig. 5. Slow spiral trajectory tracking in Scenario 1.

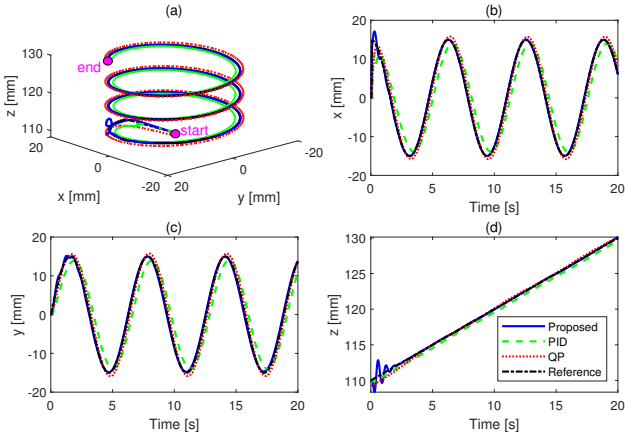

Fig. 6. Fast spiral trajectory tracking in Scenario 1.

2) Scenario 2 [With Uncertainty on Young's Modulus]: The Young's modulus of the Diamond robot implemented in SOFA platform remains 150 [KPa] as in Scenario 1. However, we modify the Young's modulus of the FEM control-based robot model to 180 [KPa] to introduce a modeling uncertainty in the control design. The control performance of the three considered methods for a slow spiral trajectory tracking is depicted in Fig. 7. Due to modeling errors and without taking into account the robot dynamics, as expected the QP-based controller leads to a worse behavior in transient responses compared to the tracking results in Scenario 1. Note that a satisfactory control performance can be maintained for both PID controller and EID-based controller in case of a slow trajectory tracking. Fig. 8 presents the fast trajectory tracking results. Since the modeling error directly affects the Jacobian matrix and the inverse kinematics, the tracking performance of the PID controller and QP controller is degraded, whereas the closed-loop behavior is preserved with the proposed controller due to its effective EID-based error compensation mechanism.

For a quantitative performance analysis, we define the following integral square tracking error (ISE) index:

$$\text{ISE} = \int_0^{\Delta t} e(t)^2 dt, \tag{40}$$

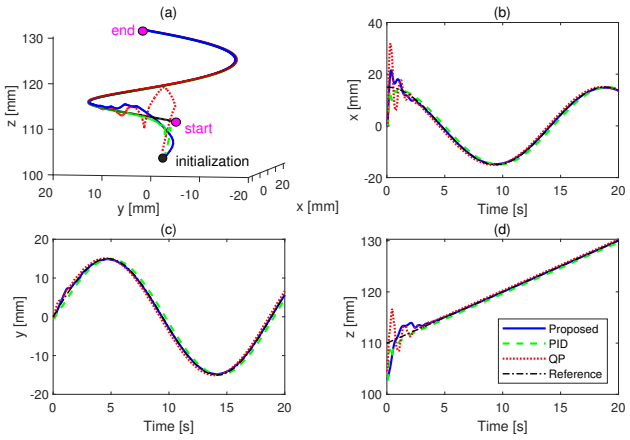

Fig. 7. Slow spiral trajectory tracking in Scenario 2.

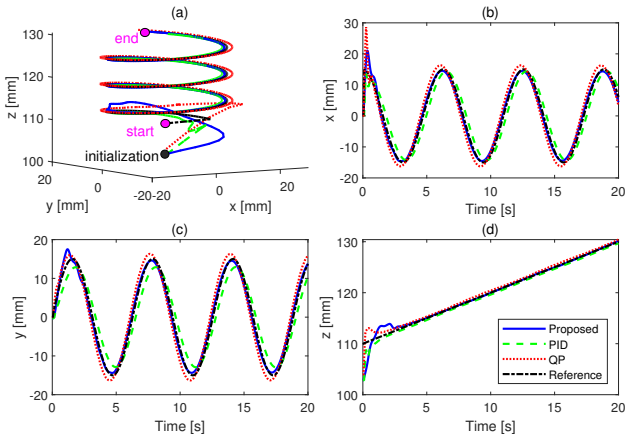

Fig. 8. Fast spiral trajectory tracking in Scenario 2.

where Δt is the tracking time. Fig. 9 summarizes the tracking performance comparisons in terms of ISE index [mm^{2}s] between the three FEM-based control methods obtained with the 3D trajectory (39) and $\Delta t = 20$ [s]. Remark that when there is no significant modeling uncertainty, the QP-based controller can provide a better tracking performance compared to the Jacobian-based controller. However, this latter seems to be more robust with respect to uncertainties than the QP-based controller. We can see also that the proposed EID-based control method provides the best tracking performance in all the test scenarios.

To reveal the insights of the EID-based controller (16) for tracking purposes, we point out the specific role of each involved control component, *i.e.*, feedback control u_{fb}, feedforward control u_{ff}, and disturbance-compensation based control u_{dc}. To this end, we reconsider Scenario 2 with a fast trajectory tracking task, decomposed into three phases:

- Phase 1: From 0 [s] to 13 [s] with only feedback control, *i.e.*, controller (16) with $u_{ff} = 0$ and $u_{dc} = 0$.
- Phase 2: From 13 [s] to 23 [s] with feedback and feedforward control, *i.e.*, controller (16) with $u_{dc} = 0$.
- Phase 3: From 23 [s] to 23 [s] with the complete EID-based controller (16).

The tracking control result along the $y-$axis direction is shown

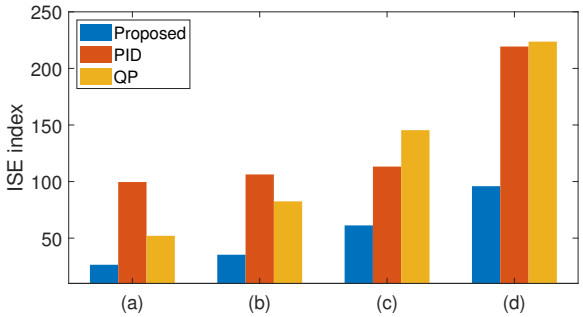

Fig. 9. Summary of the ISE performance comparisons. (a) Slow tracking without uncertainty. (b) Fast tracking without uncertainty. (c) Slow tracking with uncertainty. (d) Fast tracking with uncertainty.

in Fig. 10. During Phase 1, the tracking is performed with significant errors in amplitude and in phase. Integrating the feedforward control action in Phase 2 can only improve the phase error since the amplitude error is still observed due to the modeling uncertainty. Using the EID-based control law (16) in Phase 3, the amplitude error can be also significantly reduced with the error-compensation term u_{dc}. Hence, the proposed method allows to achieve an effective fast (and slow) tracking control for soft robots despite the modeling errors.

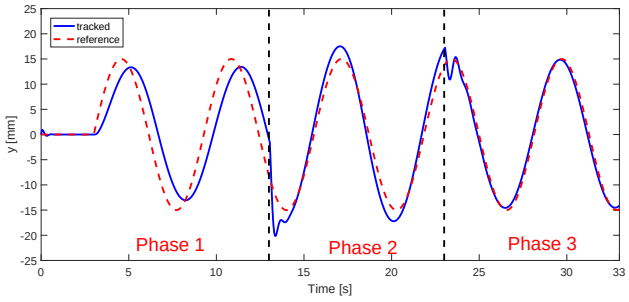

Fig. 10. Three-phase fast trajectory tracking along the $y-$axis in Scenario 2.

B. Experimental Validations

Hereafter, we present the tracking control results, experimentally obtained with the Trunk robot shown in Fig. 11.

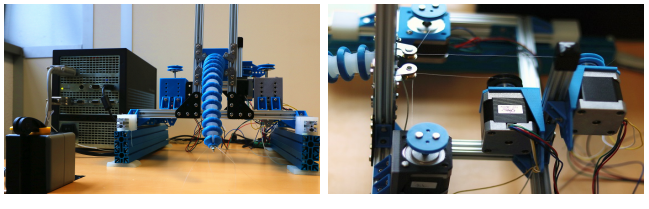

(a) (b)

Fig. 11. Trunk robot. (a) Robot platform, (b) Stepper motors.

1) Hardware Setup: The silicone Trunk robot is composed of 14 segments to make it highly deformable. This soft robot driven by four stepper motors via cables mounted on the robot body to guarantee the accessibility of each direction in the workspace. The position of the end-effector, *e.g.*, system output, is measured

by a Polhemus Liberty magnetic motion tracking sensor. The weight of the Trunk robot is 40 [g] and its length is 195 [mm] in the initial position. The FEM model of this robot has 1944 nodes, leading to 3324 state variables. After performing the POD model reduction, a reduced four-order dynamical Trunk robot model can be obtained for control design. Since the workspace of the Trunk robot is a surface, then it is sufficient to determine the position of the end-effector with a 2D reference trajectory. For tracking control purposes, we consider the spiral trajectory

$$x(t) = 0.2t\cos(\omega t), \quad y(t) = 0.2t\sin(\omega t), \tag{41}$$

with $\omega = 1$ [rad/s], corresponding to a fast trajectory tracking. Note that the linear speed of the spiral reference is continuously increasing according to the radius, making the tracking task more challenging.

2) Tracking Control Performance: For this trajectory tracking, we examine the experimental results obtained with two *dynamic* control methods: Jacobian-based PID control and EID-based control. Fig. 12 depicts the evolutions of the end-effector position tracking in the $xy-$plane, performed by both considered controllers. We can see clearly that compared to Jacobian-based PID control, the proposed EID-based control method provides a significant improvement in terms of tracking performance. The tracking performance along $x-$axis and $y-$axis directions, and the corresponding force control inputs obtained with the spiral reference trajectory (41) are given in Fig. 13. Observe in Figs. 13(c) and (d) that due to the effects of the feedforward action, the proposed EID-based controller provides a faster response with respect to the Jacobian-based PID controller, which allows for a better dynamic tracking performance as shown in Figs. 13(a) and (b). We can also see in Figs. 13(c) and (d) that the control inputs of both controllers start at the same values corresponding to the robot equilibrium point. Moreover, there is only a small amplitude difference concerning the $x-$axis force control inputs. However, along the $y-$axis the proposed EID-based controller provides a larger control action to better compensate the time-varying disturbance due to the gravity effect, which improves the control precision performance as indicated in Fig. 12. For quantitative comparison purposes, the ISE indices, defined in (40), are computed for both EID-based control and Jacobian-based PID control over a time duration $\Delta t = 22$ [s] as 153.3 [mm^{2}s] and 778.9 [mm^{2}s], respectively. For this experimental test, we can note a tracking performance improvement of about 80% in terms of ISE index. The validation videos can be found at the address: https://bit.ly/2VVwtLn.

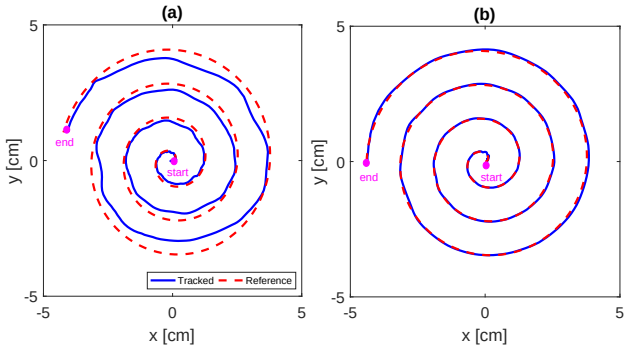

Fig. 12. Experimental results of spiral trajectory tracking control. (a) Jacobian-PID control. (b) Proposed EID-based control.

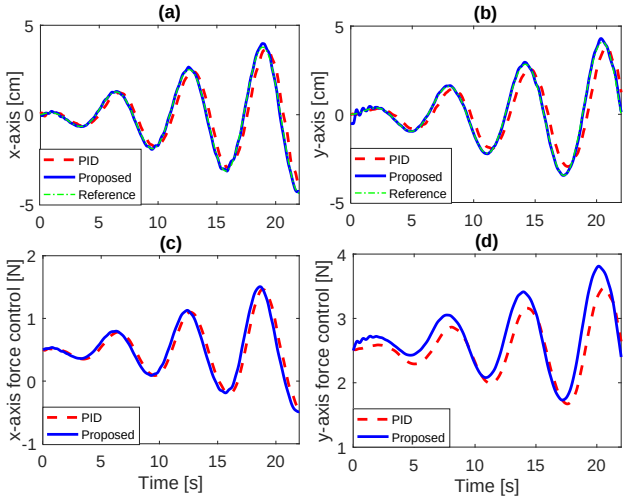

Fig. 13. Comparison of spiral trajectory tracking control. (a) Tracking performance along $x-$axis. (b) Tracking performance along $y-$axis. (c) Force control input in $x-$axis direction. (d) Force control input in $y-$axis direction.

VI. Concluding Remarks

A dynamic FEM model-based framework has been proposed for the tracking control of soft robots. For the control design, the large-scale FEM robot model is effectively reduced with a POD model reduction method. Using an EID approach, we propose an observer-based tracking control structure including three components, *i.e.*, feedback control, feedforward control, error-compensation control. This control structure allows for an effective tracking control performance despite the presence of modeling uncertainty and unknown disturbances. To improve the closed-loop responses, the concept of LMI regions is exploited together with an ℓ_∞ control design via Lyapunov stability theory. The effectiveness of the proposed control method has been first demonstrated with high-fidelity SOFA simulations performed on a Diamond soft robot. Then, experimental validations have been also carried out with a Trunk robot. Under the considered experimental conditions, the proposed control method shows a clear tracking performance improvement compared to the existing Jacobian-PID control method, *i.e.*, about 80% of improvement in terms of ISE index. Future works focus on extending the proposed method using linear parameter varying (LPV) framework and generalized proportional integral observer structures to deal with nonlinearities and modeling uncertainties caused by large deformations of soft robots. Extensions of the proposed results for the tracking control of soft robots in interaction with an unstructured environment are another promising direction.

Appendix A
Proof of Theorem 1

By Lemma 1, we can show that LMI conditions (31), (32) and (33) (respectively (34), (35) and (36)) guarantee that the eigenvalues of the dynamic matrix $\bar{A}_c$ of the tracking error system (25) (respectively $\bar{A}_o$ of the estimation error system

(23)) are confined in the LMI region $\mathscr{D}_c(r_c, \theta_c, \alpha_c)$ (respectively $\mathscr{D}_o(r_o, \theta_o, \alpha_o)$).

Pre- and postmultiplying inequality (31) with $P = X^{-1}$ while considering (38), it follows that

$$\mathrm{He}\left(P\bar{A}_c + \alpha_c P\right) \prec 0. \tag{42}$$

Let us denote

$$\Pi_c = \mathrm{He}\left(P\bar{A}_c + \alpha_c P\right), \quad \Pi_o = \mathrm{He}\begin{bmatrix} \mathscr{A}_o + \alpha_c Q & QB_{od} \\ 0 & -\alpha_c \nu I \end{bmatrix}.$$

Note that $\Pi_o \prec 0$ and $\Pi_c \prec 0$ due to conditions (30) and (42), respectively. Since Π_c only depends on the control gain K_c and matrix P, and Π_o only depends on the observer gain L_o and matrix Q, there always exists a positive scalar $\tau > 0$, sufficiently small, such that [42]

$$\Pi_o \preceq \tau \Phi^\top \Pi_c^{-1} \Phi, \tag{43}$$

with $\Phi = \begin{bmatrix} PB_o & PB_{cd} \end{bmatrix}$. By Schur complement lemma [43], we can prove that condition (43) is equivalent to

$$\begin{bmatrix} \tau\Pi_c & \tau\Phi \\ \star & \Pi_o \end{bmatrix} \preceq 0. \tag{44}$$

From the definitions of Π_c, Π_o, and Φ, condition (44) can be rewritten as

$$\mathrm{He}\begin{bmatrix} \tau P(\bar{A}_c + \alpha_c I) & \tau P B_o & \tau P B_{cd} \\ 0 & Q(\bar{A}_o + \alpha_c I) & QB_{od} \\ 0 & 0 & -\alpha_c \nu I \end{bmatrix} \preceq 0. \tag{45}$$

To study the stability of the extended closed-loop system (26), we consider a Lyapunov function candidate as

$$V(\tilde{x}) = \tilde{x}^\top \mathrm{diag}(\tau P, Q)\tilde{x}. \tag{46}$$

Now, pre- and postmultiplying (45) with $\begin{bmatrix} \tilde{x}^\top & d_{\dot{q}}^\top \end{bmatrix}^\top$ and its transpose, the following condition can be obtained after some algebraic manipulations:

$$\dot{V}(\tilde{x}) \leq -2\alpha_c (V(\tilde{x}) - \nu d_{\dot{q}}^\top d_{\dot{q}}), \tag{47}$$

where $\dot{V}(\tilde{x})$ is the time derivative of the Lyapunov function (46) along the trajectory of the closed-loop system (26). From the relation of vector-norms, inequality (47) implies that

$$\dot{V}(\tilde{x}) \leq -2\alpha_c \left(V(\tilde{x}) - \nu \|d_{\dot{q}}\|_\infty^2\right). \tag{48}$$

Applying the comparison lemma [44, Lemma 3.4] to (48), it follows that

$$V(\tilde{x}(t)) \leq e^{-2\alpha_c t} V(\tilde{x}(0)) + \nu \|d_{\dot{q}}\|_\infty^2. \tag{49}$$

Note that

$$\alpha_1 \|\tilde{x}\|^2 \leq V(\tilde{x}) \leq \alpha_2 \|\tilde{x}\|^2, \tag{50}$$

with $\alpha_1 = \lambda_{\min}\left(\mathrm{diag}(\tau P, Q)\right)$ and $\alpha_2 = \lambda_{\max}\left(\mathrm{diag}(\tau P, Q)\right)$. It follows from (49) and (50) that

$$\|\tilde{x}\| \leq \sqrt{\frac{\alpha_2}{\alpha_1}} e^{-\alpha_c t} \|\tilde{x}(0)\| + \sqrt{\frac{\nu}{\alpha_1}} \|d_{\dot{q}}\|_\infty,$$

which guarantees Property (P1), *i.e.*, the input-to-state stability of system (26) with respect to any disturbance $d_{\dot{q}} \in \mathscr{B}_\infty$.

Let us consider the definition of the performance output z in (27). Pre- and postmultiplying inequality (37) with $\mathrm{diag}(P, I, I)$, it follows that

$$\begin{bmatrix} \mathrm{diag}(P, Q) & F^\top \\ \star & \mu I \end{bmatrix} \succeq 0. \tag{51}$$

Applying Schur complement lemma and congruence transformation [43] to inequality (51), it follows that

$$\mu \mathrm{diag}(\tau P, Q) - F^\top F \succeq 0, \tag{52}$$

with $\tau > 0$. Pre- and postmultiplying condition (52) with $\tilde{x}^\top$ and its transpose yields

$$\|z\|^2 \leq \mu V(\tilde{x}). \tag{53}$$

From (49) and (53), we can deduce that

$$\|z(t)\| \leq \sqrt{\mu V(\tilde{x}(0))} e^{-\alpha_c t} + \sqrt{\nu\mu} \|d_{\dot{q}}\|_\infty. \tag{54}$$

For any initial condition $\tilde{x}(0)$ and any bounded signal $d_{\dot{q}}$, it follows from (54) that

$$\lim_{t \to \infty} \sup \|z(t)\| \leq \gamma \|d_{\dot{q}}\|_\infty,$$

which guarantees Property (P2). This concludes the proof.

REFERENCES

[1] G. Bao, H. Fang, L. Chen, Y. Wan, F. Xu, Q. Yang, and L. Zhang, "Soft robotics: Academic insights and perspectives through bibliometric analysis," *Soft Robot.*, vol. 5, no. 3, pp. 229–241, 2018.

[2] D. Rus and M. Tolley, "Design, fabrication and control of soft robots," *Nature*, vol. 521, no. 7553, pp. 467–475, 2015.

[3] C. Majidi, "Soft robotics: A perspective, current trends and prospects for the future," *Soft Robot.*, vol. 1, no. 1, pp. 5–11, 2014.

[4] E. Coevoet *et al.*, "Software toolkit for modeling, simulation, and control of soft robots," *Adv. Robot.*, vol. 31, no. 22, pp. 1208–1224, 2017.

[5] G. Gerboni, A. Diodato, G. Ciuti, M. Cianchetti, and A. Menciassi, "Feedback control of soft robot actuators via commercial flex bend sensors," *IEEE/ASME Trans. Mechatron.*, vol. 2, no. 4, pp. 81–88, 2017.

[6] T. Thuruthel, Y. Ansari, E. Falotico, and C. Laschi, "Control strategies for soft robotic manipulators: A survey," *Soft Robot.*, vol. 5, no. 2, pp. 149–163, 2018.

[7] W. Liang, J. Cao, Q. Ren, and J. Xu, "Control of dielectric elastomer soft actuators using antagonistic pairs," *IEEE/ASME Trans. Mechatron.*, vol. 24, no. 6, pp. 2862–2872, 2019.

[8] C. Duriez, "Control of elastic soft robots based on real-time finite element method," in *IEEE Int. Conf. Robot. Autom.*, 2013, pp. 982–987.

[9] E. Coevoet, A. Escande, and C. Duriez, "Soft robots locomotion and manipulation control using FEM simulation and quadratic programming," in *IEEE Int. Conf. Soft Robot.*, 2019, pp. 739–745.

[10] T. Bieze, A. Kruszewski, B. Carrez, and C. Duriez, "Design, implementation, and control of a deformable manipulator robot based on a compliant spine," *Int. J. Rob. Res.*, vol. 39, no. 14, pp. 604–619, 2020.

[11] A. Marchese, R. Tedrake, and D. Rus, "Dynamics and trajectory optimization for a soft spatial fluidic elastomer manipulator," *Inter. J. Robot. Res.*, vol. 35, no. 8, pp. 1000–1019, 2016.

[12] V. Vikas, E. Cohen, R. Grassi, C. Sözer, and B. Trimmer, "Design and locomotion control of a soft robot using friction manipulation and motor–tendon actuation," *IEEE Trans. Robot.*, vol. 32, no. 4, pp. 949–959, 2016.

[13] M. Thieffry, A. Kruszewski, T.-M. Guerra, and C. Duriez, "Trajectory tracking control design for large-scale linear dynamical systems with applications to soft robotics," *IEEE Trans. Control Syst. Technol.*, vol. 29, no. 2, pp. 556–566, 2021.

[14] J. Cao, W. Liang, Y. Wang, H. Lee, J. Zhu, and Q. Ren, "Control of a soft inchworm robot with environment adaptation," *IEEE Trans. Indus. Electron.*, vol. 67, no. 5, pp. 3809–3818, 2020.

[15] G. Fang, X. Wang, K. Wang, K. Lee, J. Ho, H. Fu, D. Fu, and K. Kwok, "Vision-based online learning kinematic control for soft robots using local Gaussian process regression," *IEEE Robot. Autom. Lett.*, vol. 4, no. 2, pp. 1194–1201, 2019.

[16] H. Wang, B. Yang, Y. Liu, W. Chen, X. Liang, and R. Pfeifer, "Visual servoing of soft robot manipulator in constrained environments with an adaptive controller," *IEEE/ASME Trans. Mechatron.*, vol. 22, no. 1, pp. 41–50, 2016.

[17] P. Hyatt, D. Kraus, V. Sherrod, L. Rupert, and N. Day, "Configuration estimation for accurate position control of large-scale soft robots," *IEEE/ASME Trans. Mechatron.*, vol. 24, no. 1, pp. 88–99, 2019.

[18] A. Bajo, R. Goldman, and N. Simaan, "Configuration and joint feedback for enhanced performance of multi-segment continuum robots," in *IEEE Int. Conf. Robot. Autom.*, 2011, pp. 2905–2912.

[19] A. Marchese and D. Rus, "Design, kinematics, and control of a soft spatial fluidic elastomer manipulator," *Int. J. Robot. Res.*, vol. 35, no. 7, pp. 840–869, 2016.

[20] T. Thuruthel, E. Falotico, F. Renda, and C. Laschi, "Model-based reinforcement learning for closed-loop dynamic control of soft robotic manipulators," *IEEE Trans. Robot.*, vol. 35, no. 1, pp. 124–134, 2018.

[21] H. Sadati, E. Naghibi, I. Walker, K. Althoefer, and T. Nanayakkara, "Control space reduction and real-time accurate modeling of continuum manipulators using ritz and Ritz–Galerkin methods," *IEEE Robot. Autom. Lett.*, vol. 3, no. 1, pp. 328–335, 2017.

[22] C. Della Santina, R. Katzschmann, A. Bicchi, and D. Rus, "Model-based dynamic feedback control of a planar soft robot: Trajectory tracking and interaction with the environment," *Int. J. Robot. Res.*, vol. 39, no. 4, pp. 490–513, 2020.

[23] R. Webster and B. Jones, "Design and kinematic modeling of constant curvature continuum robots: A review," *Int. J. Rob. Res.*, vol. 29, no. 13, pp. 1661–1683, 2010.

[24] C. Best, M. Gillespie, P. Hyatt, L. Rupert, V. Sherrod, and M. Killpack, "A new soft robot control method: Using model predictive control for a pneumatically actuated humanoid," *IEEE Robot. Autom. Mag.*, vol. 23, no. 3, pp. 75–84, 2016.

[25] D. Bruder, B. Gillespie, D. Remy, and R. Vasudevan, "Modeling and control of soft robots using the Koopman operator and model predictive control," *arXiv preprint arXiv:1902.02827*, 2019.

[26] G. Zheng, "Control of a silicone soft tripod robot via uncertainty compensation," *IEEE Robot. Autom. Lett.*, vol. 5, no. 2, pp. 1–7, 2020.

[27] F. Angelini, C. Santina, M. Garabini, M. Bianchi, G. Gasparri, G. Grioli, M. Catalano, and A. Bicchi, "Decentralized trajectory tracking control for soft robots interacting with the environment," *IEEE Trans. Robot.*, vol. 34, no. 4, pp. 924–935, 2018.

[28] Z.-Q. Tang, H.-L. Heung, K.-Y. Tong, and Z. Li, "Model-based online learning and adaptive control for a "human-wearable soft robot" integrated system," *Int. J. Robot. Res.*, p. 0278364919873379, 2019.

[29] K.-J. Bathe, *Finite Element Procedures*. Klaus-Jurgen Bathe, 2006.

[30] C. Laschi, M. Cianchetti, B. Mazzolai, L. Margheri, M. Follador, and P. Dario, "Soft robot arm inspired by the octopus," *Adv. Robot.*, vol. 26, no. 7, pp. 709–727, 2012.

[31] K. de Payrebrune and O. O'Reilly, "On constitutive relations for a rod-based model of a pneu-net bending actuator," *Extreme Mech. Lett.*, vol. 8, pp. 38–46, 2016.

[32] J. Chenevier, D. Gonzalez, J. V. Aguado, F. Chinesta, and E. Cueto, "Reduced-order modeling of soft robots," *PloS One*, vol. 13, no. 2, 2018.

[33] M. Thieffry, A. Kruszewski, C. Duriez, and T.-M. Guerra, "Control design for soft robots based on reduced-order model," *IEEE Robot. Autom. Lett.*, vol. 4, no. 1, pp. 25–32, 2018.

[34] J.-H. She, X. Xin, and Y. Pan, "Equivalent-input-disturbance approach–analysis and application to disturbance rejection in dual-stage feed drive control system," *IEEE/ASME Trans. Mechatron.*, vol. 16, no. 2, pp. 330–340, 2010.

[35] Z. Wang, J. She, Z.-T. Liu, and M. Wu, "Modified equivalent-input-disturbance approach to improving disturbance-rejection performance," *IEEE Trans. Indus. Electron.*, pp. 1–1, 2021.

[36] A. Antoulas, *Approximation of Large-Scale Dynamical Systems*. SIAM, Philadelphia, 2005.

[37] P. Benner, M. Ohlberger, A. Cohen, and K. Willcox, *Model Reduction and Approximation: Theory and Algorithms*. SIAM, Philadelphia, 2017.

[38] S. Prajna, "POD model reduction with stability guarantee," in *IEEE Int. Conf. Decision Control*, vol. 5, 2003, pp. 5254–5258.

[39] D. Koenig, "Unknown input proportional multiple-integral observer design for descriptor systems: application to state and fault estimation," *IEEE Trans. Autom. Control*, vol. 50, no. 2, pp. 212–217, 2005.

[40] M. Chilali, P. Gahinet, and P. Apkarian, "Robust pole placement in LMI regions," *IEEE Trans. Autom. Control*, vol. 4, no. 12, pp. 257–270, 1999.

[41] J. Löfberg, "YALMIP: A toolbox for modeling and optimization in Matlab," in *IEEE Int. Symp. Comput. Aided Control Syst. Des.*, Taipei, 2004, pp. 284–289.

[42] J. Yoneyama, M. Nishikawa, H. Katayama, and A. Ichikawa, "Output stabilization of Takagi–Sugeno fuzzy systems," *Fuzzy Sets Syst.*, vol. 111, no. 2, pp. 253–266, 2000.

[43] S. Boyd, L. El Ghaoui, E. Feron, and V. Balakrishnan, *Linear Matrix Inequalities in System and Control Theory*. Philadelphia, PA: SIAM, 1994, vol. 15.

[44] H. Khalil, *Nonlinear Systems*, 3rd, Ed. Prentice Hall, 2002.

Shijie Li received the B.Sc. degree from the University of Science and Technology of China, China, in 2016, and the M.Sc. degree from Moscow State University, Russia, in 2019. He is working toward the Ph.D. degree in automatic control at Université Polytechnique des Hauts-de-France, Valenciennes, France. He a member of the LAMIH laboratory, UMR CNRS 8201, Valenciennes, and the DEFROST INRIA team, CRIStAL laboratory, UMR CNRS 9189, Villeneuve d'Ascq, France. His research topic focuses on dynamic control of soft robots.

Alexandre Kruszewski is a Full Professor at the École Centrale de Lille, France. He received the Ph.D. degree in automatic control from the University of Valenciennes et du Hainaut-Cambrésis, Valenciennes, France, in 2006, and the HDR degree from the University of Lille, France, in 2017.

He is with the DEFROST team, CRIStAL Laboratory, UMR 9189, Villeneuve d'Ascq. His main researches deal with the robust stabilization of polytopic systems with application to soft robots.

Thierry-Marie Guerra is currently a Full Professor at Université Polytechnique Hauts-de-France, France. He received his PhD degree in automatic control in 1991 and the HDR in 1999. From 2010 to 2019, he was the head of the laboratory LAMIH UMR CNRS 8201. Since July 2020, he is member of the Technical Board (Coordinating Committee Chair CC 3 - Computers, Cognition and Communication) of IFAC (International Federation of Automatic Control). From 2014 to 2020 he served as chair of the Technical Committee 3.2 "Computational Intelligence in Control" of IFAC. He is an Area Editor of the international journals: Fuzzy Sets & Systems and IEEE Transactions on Fuzzy Systems. His major research fields and topics of interest are nonlinear control, LPV, Takagi-Sugeno models control and observation, LMI constraints, nonlinear Lyapunov functions and applications to mobility, soft robotics and disabled persons.

Anh-Tu Nguyen (M'18, SM'21) is an Associate Professor at the INSA Hauts-de-France, Université Polytechnique Hauts-de-France, Valenciennes, France. He received the degree in engineering and the M.Sc. degree in automatic control from Grenoble Institute of Technology, France, in 2009, and the Ph.D. degree in automatic control from the University of Valenciennes, Valenciennes, France, in 2013. He is an Associate Editor for the IEEE Transactions on Intelligent Transportation Systems, the IET Journal of Engineering, and an Early Career Advisory Board member of the IFAC journal Control Engineering Practice. Dr. Nguyen's research interests include robust control and estimation, human-machine shared control with a strong emphasis on mechatronics applications.